Experimental investigation of organic Rankine cycle performance using alkanes or hexamethyldisiloxane as a working fluid

Wameedh Khider Abbas Abbas[A], Elmar Baumhögger[A], Jadran Vrabec[B]

[A] Thermodynamics and Energy Technology, University of Paderborn, Warburger Straße 100, 33098 Paderborn, Germany

[B] Thermodynamics and Process Engineering, Ernst-Reuter-Platz 1, 10587 Berlin, Germany

---

Abstract

An experimental investigation of the organic Rankine cycle (ORC) is carried out using butane, pentane, cyclopentane or hexamethyldisiloxane as a working fluid. Thermal and exergy efficiencies are used to assess system performance over a wide range of heat source temperature, turbine inlet pressure and superheating degree. The results indicate that both of these efficiencies increase with rising heat source temperature and turbine inlet pressure. Under the present experimental conditions, without using an optimized turbine, the highest thermal efficiency and exergy efficiency are 8.0% and 25.2%, respectively. The results show that hexamethyldisiloxane is a better working fluid than the alkanes under all experimental conditions. Moreover, it is found that a small superheating degree may be beneficial. Exergy loss analysis indicates that most of the loss occurs in the evaporator and that a working fluid with a high critical temperature is advantageous for ORC systems driven by a heating cycle with a heat transfer fluid.

Keywords: Thermal efficiency, exergy efficiency, heat source temperature, working fluid, alkane, siloxane.

Corresponding author: Jadran Vrabec, tel.: +493031422755, E-mail: vrabec@tu-berlin.de

1. Introduction

Power supply is at the core of modern societies and it is clear that the demand for more is poised to further increase in the decades to come due to population growth and development. While the large majority of electrical energy stems from fossil sources, the associated release of carbon dioxide is not sustainable. Now, it is widely accepted that traditional energy conversion processes must be curbed and alternatives are urgently needed [1,2]. One option that can yield clean, eco-friendly power is the organic Rankine cycle (ORC). This technology can be driven by any heat source, such as geothermal, biomass, solar-thermal or industrial waste heat, utilizing various temperature levels [3].

Currently, there are more than 2700 ORC projects with power generation units ranging from a few kilowatts to several dozen megawatts and the total capacity is above 4 GW. Since 2016, the ORC market has witnessed a significant growth, as more than 850 units were added with a capacity of about 1.18 GW. The total capacity can be divided into geothermal (77.4 %), waste heat recovery (11.6 %) and biomass (10.1 %), while other applications have a minor percentage: waste-to-energy (0.7 %), solar (0.2 %) and remote (0.03 %) [4,5].

Since the emergence of ORC technology, many studies have experimentally tested its efficiency and studied different operating conditions, architectures and heat sources. Most of the published experiments were based on small-scale ORC or prototypes [6]. Park et al. [7] presented a comprehensive review of experimental investigations from 2009 until 2018. They reported that R245fa, R123 and R134a were the most widely employed working fluids and that the majority of published works examined ORC systems with a turbine power output below 10 kW. The investigated ORC systems were thus on a small scale and the applied heat source temperature was either constant or varied over a small range.

In the subsequent short review of experimental works from 2018 until today, we also found that most researchers have studied on small-scale ORC with a turbine power output between 1 and 50 kW. It was focused on system performance in terms of thermal, exergy and turbine efficiencies as well as heat characteristics. The thermal efficiency is usually considered as the most suitable indicator because it is the ratio between the net power output and the heat flow rate supplied to the evaporator.

Mascuch et al. [8] carried out an experimental study on a kilowatt-scale biomass-fired ORC utilizing hexamethyldisiloxane (MM) as a working fluid with a turbine inlet temperature of 192 °C. The authors showed that the isentropic efficiency of the turbine was between 28% and 52%,

which led to a low thermal efficiency of 2.5%. Feng et al. [9] considered R245fa as a working fluid and explored the performance of basic and regenerative ORC. The maximum thermal efficiency was 5.5% and it was found that the evaporator was critical with respect to exergy loss, indicating that system performance can be improved by decreasing the temperature difference between the heat source and the turbine inlet. Gao et al. [10] investigated a R290-based ORC experimentally by varying evaporation pressure and pressure drop, achieving a maximum thermal efficiency of 6.78%. Wang et al. [11] studied a 1 kW-scale ORC with R290 as a working fluid in the context of cold energy utilization. System performance was evaluated at a heat source temperature in the range of 20-55 °C and the maximum thermal efficiency was 6.49%. Araya et al. [12] experimentally compared R1233zd(E) and R245fa as working fluids with respect to system performance. They reported that the highest thermal efficiency was 5.0% when utilizing R1233zd(E) at a heat source temperature of 85.7 °C. Kaczmarzyk et al. [13] presented an experimental investigation on a small-scale ORC system which uses a biomass boiler as a heat source. They utilized a radial-flow turbine as expander device and recorded an isentropic turbine efficiency in the range from 52% to 71%, leading to a maximum thermal efficiency of 6.5%. İpek et al. [14] investigated the performance of a low-temperature ORC system to recover heat from a gas turbine using R134a as a working fluid. They found that the heat source temperature in the range 86-88 °C was optimal to reach the maximum system performance in terms of thermal efficiency, expansion ratio and turbine power output. The highest achieved thermal efficiency was 6.84% at a heat source temperature of 86.5°C. Wu et al. [15] studied system performance in terms of thermal and exergy efficiencies and exergy loss using R245fa as a working fluid. They reported that the highest thermal and exergy efficiencies were 2.54% and 8.09%, respectively. The authors also found that most of the exergy loss occurred in the evaporator (58.38%). Fatigati et al. [6] followed an experimental approach to evaluate turbine power output and thermal efficiency of a small-scale ORC for different flow rates of R245fa working fluid. Their system generated turbine power output in the range of 200-500 W, while the thermal efficiency was 4-6%. The authors pointed out that the low thermal efficiency was due to the poor efficiency of the turbine, which underlines that the latter is a crucial parameter for ORC system performance. Qui and Entchev [16] carried out an experimental study with a micro-combined heat and power ORC system using R1223zd(E) and n-pentane as a working fluid. The thermal efficiency of both working fluids was tested at a turbine inlet temperature of 135-136 °C and a pressure ratio of 3.65, leading to a maximum thermal efficiency of 5.6% and 5.3%, respectively. Carraro et al. [17] investigated the

performance of a biomass-fired micro-ORC system using R245fa as a working fluid that had its maximum performance for a heat source temperature of 150 °C. They reported that the electrical efficiency (ratio of net electric power to absorbed heat flow) and turbine efficiency were 7.4% and 57%, respectively. Qiu et al. [18] tested an ORC-based micro-combined heat and power unit for residential applications. They selected pentane as a working fluid to study turbine power output and cycle efficiency. Their simulation results showed that their system may reach a cycle efficiency of 10%, which was higher than the experimental results.

The present literature review confirms that ORC systems with a turbine power of up to 15 kW are characterized by a low thermal efficiency, which in turn is attributed to the poor turbine efficiency at this power scale. Most research focused on specific working fluids and the measurements were done at a specific heat source temperature or over a narrow range. Rather few parameters were varied in a given work. Studies dealing with alkanes and siloxanes as working fluids are very limited. As far as the authors are aware, there is no experimental study that tests and compares the performance of several alkanes and a siloxane under a wide range of operating conditions. Table 1 gives a summary of the present literature review.

Generally, there is a gap between theoretical and practical work looking at ORC system performance. The reason is that theoretical studies depend on calculations with simulation programs to assess different working fluids and varying operating conditions. However, most of these theoretical studies assumed parameters at optimal values that require well-designed components that are different to be put in practice [19,20].

The novelty of this work is that the performance of ORC system is studied experimentally in terms of thermal and exergy efficiencies using four working fluids over a wide range of heat source temperature, turbine inlet pressure and superheating degree. Turbine efficiency, enthalpy drop across the turbine and exergy loss are investigated as well. It attempts to fill this gap with an experimental investigation of ORC system technology over a wide range of operating conditions, where butane, pentane, cyclopentane and MM were employed as a working fluid.

2. Materials and methods

2.1. ORC test rig

The present test rig facility is a part of the cascaded two-ORC system (CORC) that was designed and built at the University of Paderborn. It formed the basis for several studies. The first one dealt with the installation of the system and explained its main components and operation

process, outlining a preliminary test using two working fluids [22]. The second investigation looked at CORC operation with varying working fluids, where thermal efficiency, heat transfer properties and pinch point temperature difference were assessed [25]. The third paper described a simulation study of the same system considering alkanes and 31 low-GWP refrigerants [26].

The CORC consists of two cascaded ORC, namely the high-temperature cycle (HT-ORC) and the low-temperature cycle (LT-ORC). Each cycle consists of the main components of an ORC system i.e. pump, evaporator, turbine and condenser. According to the design of the test rig, the HT-ORC can operate as a regular ORC system because it contains all main components and is directly connected to the heat source.

The ORC test rig has three main cycles, i.e. heating cycle that acts as the source, power generation cycle and cooling cycle. The process diagram and the front view of the ORC test rig are shown in Fig. 1. The system was connected to the heating cycle with a thermal power of up to 158 kW. The maximum applicable temperature was specified to be 300 °C to avoid thermal decomposition of the heat transfer fluid (Therminol 66) in the heating cycle. The ORC test rig provided a stable and controlled mass flow rate of working fluid and heat source temperature. To mitigate safety issues, the system was equipped with fast-acting controllers and valves. The system components were designed and selected to improve operating flexibility and allow for the utilization of a wide range of working fluids. Furthermore, the ORC test rig components were sized to meet demanding conditions in terms of heat source temperature, vapor pressure, mass flow rate of the working fluid, environmental and safety aspects. Consequently, the turbine was not optimized for a specific working fluid or operating conditions. The flexible design of the present ORC test rig makes it suitable for testing a large number of working fluids over a wide range of conditions. The maximum operating temperature of the system is 300 °C so that it may recover heat from several source types, such as biomass or waste heat, which can be found e.g. in cement or aluminium industries. Moreover, the ORC system is an assembly of heat exchangers, pumps and condensers that are readily available in the market such that it can be converted into a practical application quite straightforwardly. The ORC cycle and its main components are shown in Fig. 2. Tables 2 and 3 list the basic components and measuring devices of the ORC test rig.

2.2. ORC cycle

The present ORC consisted of a progressive cavity pump (M1), a plate heat exchanger as an evaporator (HE), a radial turbine as an expander (T), a six-pole synchronous generator (G) and a plate heat exchanger as a condenser (C). The pump pressurized the working fluid in the liquid state and delivered it to the evaporator (process 6-3), where it was preheated, evaporated and superheated (process 3-4). Then, the working fluid expanded through the turbine to generate power (process 4-5). After expansion, the working fluid was cooled down and liquified in the condenser by discharging heat to the ambient via the cooling cycle (process 5-6).

2.3. Heating cycle

Four flow heaters represented the heat source with a maximum thermal power of 158 kW. The electrical heaters consisted of three standard heating rods and one thyristor-controlled heating rod for specifying the heat source temperature. Electrical heaters are inherently simple to control and can be easily adjusted, which allows for the investigation of a wide range of heat source temperatures. Moreover, electrical heaters may reach a high temperature level with low operational risk and reduce the uncertainty of heat flow input. Therminol 66 was used as a heat transfer fluid due to its good thermal stability, low vapor pressure and non-corrosiveness to the components of the heating cycle. The heat transfer fluid was supplied by Fragol [27]. During the process, Therminol 66 was heated up by the electrical heaters and circulated through the heating cycle via a radial flow pump (M0) to deliver the driving heat flow to the working fluid via the heat exchanger (HE).

2.4. Cooling cycle

The role of the cooling cycle of the ORC system was to dissipate the residual heat after the expansion process. The cooling cycle was located outside of the test laboratory and consisted of an air cooler connected to a condenser (C) in the form of a plate heat exchanger. The working fluid in the cooling cycle was a binary ethylene-glycol/water mixture that was circulated with a pump (M2). The residual heat flow after expansion was absorbed by the liquid ethylene-glycol/water mixture and rejected to the ambient via the air cooler.

2.5. Working fluid selection

The selection of the working fluid is of key importance for the performance and is the first step of designing an ORC system. It should address several considerations, including

thermodynamic properties, thermal stability, material compatibility, inertness with respect to the employed materials, heat transfer characteristics, specific heat, cost, safety aspects and environmental considerations (GWP and ODP) [28,29]. The working fluids selected in this work have a low GWP and zero ODP. MM is environmentally friendly and does not harm the ozone layer, while the alkanes have a GWP of about 20 and zero ODP.

Alkanes have been introduced as working fluids due to environmental aspects and their desirable critical temperature, which allows for a wide range of heat source temperatures. Consequently, butane and pentane are utilized in some commercial ORC systems [30]. Siloxanes have been introduced as a working fluid of ORC systems with a high heat source temperature. Wang et al. [31] measured the thermal stability of siloxanes and reported that they are appropriate working fluids for high-temperature ORC systems. In this context, a noticeable number of studies investigated the effect of different working fluid groups on ORC system performance. Li et al. [32] reported that alkanes are suitable for high-temperature waste heat recovery as well. The authors recommended working fluids with a high critical temperature for high heat source temperatures due to the high turbine inlet temperature that can be imposed during the expansion process. Uusitalo et al. [33] evaluated the impact of the critical properties of working fluids on ORC performance for alkanes and siloxanes. Their results indicated that there is a strong relationship between the thermal efficiency of the system and the critical properties of the working fluid. Loni et al. [34] presented a review of solar-driven ORC systems. They found that butane is the best option for low-temperature ORC units, while MM may be suitable for high-temperature ORC systems due to its high critical temperature, good thermal stability and thermodynamic performance. Sorgulu et al. [35] reported energy and exergy analyses of an ORC system that was integrated with drying and combustion subsystems using MM as a working fluid. Their results indicated that the energy and exergy efficiencies were 29.45% and 28.05%, respectively. Bahrami et al. [36] presented a review of low-GWP working fluids for ORC applications and pointed out that alkanes allow for a good thermodynamic performance. Pili et al. [37] reported a multi-objective optimization of an ORC system utilizing three working fluids. Their results indicated that pentane is the best option for their ORC among the selected working fluids in terms of net power output. The exergetic optimization of two-stage ORC for waste heat recovery was investigated by Braimaikis et al. [38]. They considered four alkanes and three refrigerants to explore the exergy efficiency for a heat source temperature between 100 °C and 300 °C. They reported that their system achieved the highest exergy

efficiency when utilizing cyclopentane and butane in the high-temperature ORC and the low-temperature ORC, respectively.

There is a growing body of literature that deals with the relationship between ORC system performance and the thermophysical properties of working fluids. The selection of working fluids with a high critical temperature may allow for a good thermal efficiency in low- and high-temperature ORC systems [39]. Aljundi [40] and Barse et al. [41] showed a correlation between thermal efficiency and the critical temperature of the working fluid. Braimakis et al. [38] reported that a small difference between the heat source temperature and the critical temperature of the working fluid is advantageous. In this context, Vivian et al. [42] reported that a difference of 35 °C between the heat source temperature and the critical temperature of working fluid is optimal, while Zhai et al. [43] proposed that this difference should vary between 35 °C and 50 °C.

The objective of this work was to provide practical data on the performance of a ORC using alkanes and MM as working fluids and under different conditions, including heat source temperature, turbine inlet pressure (TIP), superheating degree and pressure ratio. The relationship between system performance and critical properties of the working fluids was studied as well. The critical temperature of the four working fluids varies from 151.98 °C to 245.55 °C, while the critical pressure varies from 19.311 bar to 45.828 bar. Table 4 lists the properties of the selected working fluids. The properties of the selected working fluids are listed in Table 4.

2.6. Thermodynamic analysis

To evaluate the experimentally measured data, the ORC system was modelled on the basis of the first and second laws of thermodynamics. Thereby, it was assumed to be in a steady state and heat losses in the components were neglected. Furthermore, it was assumed that no significant pressure drop occurs in the condenser, heat exchangers or pipes and that the turbine does not exchange heat with the ambient.

For the evaluation of the measured quantities of this experimental study, working fluid properties were calculated with the REFPROP 10.0 [44] database, which rests on the most accurate equations of state, i.e the ones by Bücker et al. [45] for butane, Span et al. [46] for pentane, Gedanitz et al. [47] for cyclopentane and Thol et al. [48] for MM.

Process (1-2): Therminol 66 is heated by electrical heaters to transfer the heat flow $\dot{Q}_{HC}$ [kW] to the working fluid of the ORC via the heat exchanger HE. The heat flow [kW] can be calculated by [22]

$$\dot{Q}_{HC} = \dot{m}_{HC}\, c_p\, (T_2 - T_1) \quad (1)$$

where $\dot{m}_{HC}$ [kg/s] the mass flow rate of Therminol 66, c_p [kJ/(kg K)] its specific isobaric heat capacity and T_1 and T_2 [°C] are the inlet and outlet temperatures of the heat exchanger, respectively. The heat flow delivered by the heating cycle drives the ORC (3-4) and evaporates the working fluid. The heat flow [kW] absorbed by the working fluid is [22]

$$\dot{Q} = \dot{m}\, (h_4 - h_3) \quad (2)$$

where $\dot{m}$ is the mass flow rate of the working fluid in the ORC, h_3 and h_4 [kJ/kg] are its enthalpies at the inlet and outlet of the heat exchanger HE.

Process (4-5) represents to the expansion of the working fluid through the turbine, where the power output [kW] is given by [11]

$$\dot{W}_T = \dot{m}\, (h_4 - h_5) \quad (3)$$

where h_4 and h_5 are the enthalpies at the inlet and outlet of the turbine.

Process (5-6) refers to the condensation process of the working fluid which rejectes heat in condenser C and can be calculated by [49]

$$\dot{Q}_C = \dot{m}\, (h_5 - h_6) \quad (4)$$

where h_5 and h_6 are the enthalpies at the inlet and outlet of the condenser.

Process (6-3) represents the compression with pump M1 and the associated power [kW] can be determined as [11]

$$\dot{W}_P = \dot{m}_{HT}\, (h_3 - h_6) \quad (5)$$

where h_6 and h_3 are the enthalpies at the inlet and outlet of the pump.

The thermal efficiency [%] of the ORC can be defined as the ratio of the net power output [kW] to the heat flow input to the ORC [49]

$$\eta_{th} = \frac{\dot{W}_{net}}{\dot{Q}_{HC}} \quad (6)$$

where $\dot{W}_{net} = \dot{W}_T - \dot{W}_P$. (7)

The exergy efficiency [%] of the ORC is expressed as the ratio of net power output to exergy flow input [kW] [38]

$$\eta_{ex} = \frac{\dot{W}_{net}}{\dot{E}^{in}} \quad (8)$$

Therein, $\dot{E}^{in}$ [kW] is the exergy flow from the heat source, which was calculated by [38]

$$\dot{E}^{in} = \dot{m}_{HC}\,[(h_{in} - h_0) - T_0(s_{in} - s_0)] \quad (9)$$

where subscript 0 refers to ambient conditions, s_{in} and s_0 [kJ/(kg K)] are the corresponding entropies, while the subscript *in* refers to the inlet condition of the heat source.

The isentropic turbine efficiency [%] can be calculated by [11]

$$\eta_T = \frac{h_4 - h_5}{h_4 - h_{5s}} \quad (10)$$

where h_{5s} is the enthalpy of the working fluid at the outlet of a hypothetic isentropic turbine.

The exergy loss of component *i* [kW] can be calculated by [19]

$$\dot{I}_i = \dot{E}_i^{in} - \dot{E}_i^{out} \quad (11)$$

where $\dot{E}_i^{in}$ is the exergy flow into component *i* and $\dot{E}_i^{out}$ is the exergy flow of the outlet of component *i*.

The exergy loss percentage [%] of each component was calculated by [40]

$$X_i = \frac{\dot{I}_i}{\dot{I}_{total}} \quad (12)$$

where $\dot{I}_{total}$ is the total exergy loss [kW] in the system.

All measurements that we inserted in to Eqs. (1) to (12) to evaluate the ORC process were average values of temperature and pressure at each state point.

2.7. Parameters and operational conditions of the experiments

Heat source temperature, TIP and superheating degree were employed as parameters to investigate system performance. Thermal efficiency indicates the use of the heat source and the fraction of heat flow input that is converted into turbine power output. Therefore, it is linked to the available heat flow, which is related to heat exchanger performance. On the other hand, exergy analysis (exergy efficiency and exergy loss) addresses maximum power that can theoretically be generated by bringing the system into equilibrium with its surrounding and clarifies the exergy loss in different components of the ORC system [50]. Moreover, the turbine efficiency and enthalpy drop across the turbine were calculated because these two factors have a direct impact on the design of the turbine and the thermal efficiency of the system.

First, the performance of the ORC in terms of turbine power output, thermal efficiency and exergy efficiency was investigated over a wide range of heat source temperature. Experiments were carried out by using either butane, pentane, cyclopentane or MM as a working fluid. To avoid critical conditions, the maximum applied heat source temperature was restricted by the operating temperature of the heat exchanger and it was ensured that the turbine inlet temperature

was below the critical temperature of the working fluid. Consequently, the heat source temperature was in the range of 80-180 °C for butane, 130-230 °C for pentane, 180-280 °C for cyclopentane and 180-280 °C for MM.

Measurements were carried out according to the experimental procedure shown in the flow chart in Fig. 3. Initially, the electric heaters were turned on to bring the heat transfer fluid to the targeted heat source temperature. Then, the mass flow of Therminol 66 was gradually raised and pump M1 was switched on to transfer the working fluid to the evaporator (HE1) to absorb heat from the heating cycle. When the measuring point was changed, the electric heating power was gradually increased to raise the heat source temperature by an increment of 10 °C and the mass flow rates of Therminol 66 and the working fluid were adjusted. When the required parameters were reached, it has waited for sampling until the operation point was stable. The measured data were stored automatically with a personal computer.

Second, the heat source temperature was kept constant at the maximum applicable temperature for each working fluid, while the TIP was varied from 28 bar to 36 bar for butane, from 24 bar to 32 bar for pentane, 36 bar to 44 bar for cyclopentane and 10 bar to 18 bar for MM. Third, system performance was investigated by applying a varying superheating degree between 1 °C and 18 °C. The TIP was varied by changing the rotational speed of the pump M1. Each time the rotational speed of the pump was raised, the mass flow of the heating cycle and the heat source temperature were adjusted to meet the required values.

Finally, system performance was assessed for a varying superheating degree in the range of 1 °C to 18 °C. The heat source temperature controllers were set to the required temperature and the TIP was gradually raised, with attention to other parameters like working fluid mass flow rate. The same superheating range was measured for all working fluids, ensuring that the heat source temperature did not reach critical states.

The operating conditions and basic parameters of these experiments are listed in Table 5. They are related to design aspects of various components and the thermophysical properties of the working fluids of the present ORC system.

2.8. Uncertainties and validation

Thermodynamic calculations were based on REFPROP, which is a Helmholtz energy equation of state library provided by the National Institute of Standards and Technology, Boulder, CO. Typical uncertainties of the thermodynamic properties of the selected working fluids vary from

0.2% to 1% in terms of isobaric heat capacity, from 0.1% to 1% in terms of speed of sound, from 0.1% to 0.2% in terms of vapor pressure and from 0.2% to 0.3% in terms of density [44]. The uncertainties are larger in the region around the critical point, which was avoided in this investigation.

The uncertainties of the measuring devices of the test rig are listed in Table 6. Due to the lack of experimental investigations on ORC systems with the same working fluids and the same operating conditions, the thermal efficiency of pentane was compared with Ref. [16] for a heat source temperature of 136 °C. The thermal efficiency of butane was compared with our simulation work [26] at the same heat source temperature.

3. Results and discussion

3.1. Heat source temperature

A system performance analysis was made to identify suitable operating conditions of the present ORC. The experiments were carried out adopting butane, pentane, cyclopentane or MM as a working fluid over a heat source temperature in increments of 10 °C. The heat source temperature was in the range of 80-180 °C for butane, 130-230 °C for pentane, 180-280 °C for cyclopentane and 180-280 °C for MM.

Fig. 4 (a) depicts the variation of thermal efficiency with heat source temperature. As expected, all working fluids showed an increasing thermal efficiency with rising heat source temperature. The most pronounced increase of thermal efficiency was found for MM, while it was lowest for butane. The thermal efficiency increased from 1.9% to 5.4% for butane, from 2.1% to 6.4% for pentane, from 3.1% to 6.9% for pentane and from 3.3% to 8.0% for MM. The main reason for the enhanced thermal efficiency is that the enthalpy drop across the turbine increases with rising heat source temperature, leading to more net power output. The increase of the heat source temperature led to an increase of the heat flow input from the heating cycle, but the increasing rate of net power output outweighed the rising rate of absorbed heat so that the thermal efficiency increased gradually. In addition, a higher heat source temperature in this test allowed for a better utilization of the heat source for each working fluid.

Fig. 4 (b) depicts the variation of exergy efficiency with heat source temperature. The higher the heat source temperature, the higher the exergy efficiency for all working fluids. The

increasing trend of exergy efficiency is related to the increase of net power output rising with the heat source temperature. The highest achieved exergy efficiency was 20.3%, 22.5%, 23.5% and 25.2% by adopting butane, pentane, cyclopentane and MM, respectively.

As shown in Fig 5 (a), the enthalpy difference across the turbine increased greatly upon temperature rise from 17.91 kJ/kg to 43.9 kJ/kg, from 13.7 kJ/kg to 46.0 kJ/kg, from 17.5 kJ/kg to 47.6 kJ/kg and from 28.3 kJ/kg to 48.8 kJ/kg by adopting butane, pentane, cyclopentane and MM, respectively. Fig. 5 (b) shows the variation of turbine efficiency with heat source temperature. The results indicate that the turbine efficiency increased with heat source temperature for all working fluids. The highest turbine efficiency was 48.2%, 49.6, 50.1% and 51.1% for butane, pentane, cyclopentane and MM, respectively. Turbine efficiency and enthalpy difference are two important factors for evaluating the performance of the turbine and for the future design of a dedicated turbine.

3.2. Turbine inlet pressure

System performance was investigated for different TIP levels that were in the range of 28-36 bar for butane, 24-32 bar for pentane, 36-44 bar for cyclopentane and 10-18 bar for MM. The heat source temperature was kept constant at 180 °C for butane, 230 °C for pentane, 280 °C for cyclopentane and 280 °C for MM in these TIP variations. These heat source temperatures were selected because the system reached the highest thermal and exergy efficiencies under these conditions. The TIP was gradually increased for each working fluid by adjusting the rotation frequency of the M1 pump. The inlet pressure was maintained below the critical pressure of the given working fluid to avoid supercritical conditions. Fig. 6 (a) shows the effect of the TIP on the thermal efficiency. When the TIP rises, the thermal efficiency increases rather slightly from 3.3% to 4.7%, from 4.4% to 5.1%, from 4.8% to 5.9% and from 6.1% to 7.2% by adopting butane, pentane, cyclopentane and MM as a working fluid, respectively. The increase of the TIP led to an increase of the pressure ratio between inlet and outlet. A rising pressure ratio is related to the enthalpy drop across the turbine and more net power is produced as shown in Fig. 7 (a). In other words, the increase of the TIP resulted in an increase of the ratio of net power output to heat flow input, i.e. a better thermal efficiency.

The variation of exergy efficiency with TIP is depicted in Fig. 6 (b). It can be seen that the exergy efficiency also rises with TIP. It increased from 14.0% to 18.4%, for butane from 16.1% to 20.6% for pentane, from 17.8% to 22.3% for cyclopentane and from 18.4% to 23.1% for MM. This exergy efficiency trend is expected due to the rising enthalpy drop across the turbine

as shown in Fig. 7 (a). A higher TIP led to more net power output and better exergy efficiency. Increasing the TIP led to a better ratio of net power output to input exergy flow input.

Fig. 7 shows the effect of the TIP on the enthalpy difference across the turbine and the turbine efficiency. As the TIP increased, the enthalpy difference increased from 34.5 kJ/kg to 41.3 kJ/kg, from 33.2 kJ/kg to 41.0 kJ/kg, from 36.4 kJ/kg to 42.4 kJ/kg and from 34.3 kJ/kg to 43.7 kJ/kg for butane, pentane, cyclopentane and MM, respectively. The maximum turbine efficiency was 50.2%, 50.6%, 51.3% and 53.5% adopting butane, pentane, cyclopentane and MM, respectively.

A higher TIP required more pump power, which reduced net power output. Moreover, increasing the TIP led to a rise of the absorbed heat from the heating cycle and reduced the thermal efficiency. Consequently, the thermal efficiency in the first case (section 3.1) is higher for all working fluids than in the second case (section 3.2). The same applies to the exergy efficiency.

3.3. Superheating degree

System performance was assessed for a varying superheating degree in the range of 1 °C to 18 °C. The heat source temperature was carefully increased together with the mass flow rate of Therminol 66 to reach a targeted superheating degree. In Fig. 8 (a), it can be seen that the thermal efficiency first increases slightly with superheating degree up to a maximum and then decreases slightly for all working fluids. The highest thermal efficiency was generally at a superheating degree between 3 °C and 6 °C. MM and pentane reached the highest thermal efficiency at a superheating degree of 5 °C, while cyclopentane and butane showed the highest thermal efficiency at 6 °C and 4 °C, respectively. A further increase of the superheating degree did not have a significant effect. With the rise of the superheating degree, the ratio of net power to absorbed heat flow increased until a certain superheating degree, then the effect was reversed and that ratio fell so that the thermal efficiency decreased. These results agree with the analysis of Uusitalo et al. [33] and our previous work [26]. Uusitalo et al. recommended a small superheating degree for regular ORC (without recuperator) to achieve a better performance and to control the heat transfer in the evaporator of the ORC system. A control of heat transfer may reduce the exergy loss in the evaporator and increase thermal and exergy efficiencies.

Fig. 8 (b) depicts the variation of exergy efficiency with superheating degree. The exergy efficiency also increases with superheating degree and then decreases. As shown in Fig. 8 (b),

it reaches maximum values between 3 °C and 6 °C of superheating for all working fluids. At a superheating degree between 3 °C and 6 °C, the ratio of net power output to exergy flow input increases slightly. MM and cyclopentane reached the highest exergy efficiency at a superheating degree of 5 °C, while pentane and butane led to the highest exergy efficiency at 4 °C and 6 °C, respectively. These results agree with those of Zhou et al. [20], who found that a further increase of the superheating degree may lead to a slight decrease of the exergy efficiency. According to the impact of the superheating degree on the system performance, it is clear that the superheating degree should be controlled to be in that limited range.

3.4. Pressure ratio

Fig. 9 shows the variation of system performance with the pressure ratio, which is given in the form of TIP divided by the critical pressure. The results indicate that both thermal end exergy efficiencies increase with the pressure ratio for all working fluids. It can be seen that MM reached the highest thermal and exergy efficiencies at a pressure ratio of 0.9, while cyclopentane, pentane and butane reached the highest thermal efficiency at a pressure ratio of 0.91, 0.88 and 0.89, respectively, which is rather close to the critical pressure of the given working fluid. The main reason is that the increase of the TIP led to an increase of the pressure difference between the inlet and outlet of the turbine and thus a large enthalpy difference, which raised the net power output and increased thermal and exergy efficiencies.

3.5. Critical properties

Fig. 10 (a) shows the relation between the critical properties of the working fluids and the thermal and exergy efficiencies. It can be seen that there is a clear relation between system performance and the critical temperature of the working fluid, where thermal and exergy efficiencies attained better values with increasing critical temperature. The higher the critical temperature of the working fluid, the higher the efficiencies. MM with the highest critical temperature achieved the best thermal and exergy efficiencies under all experimental conditions. The mean reason is that working fluids with a high critical temperature allow for a high turbine inlet temperature and evaporation temperature, which resulted in a large enthalpy difference across the turbine. In addition, the use of a working fluid with a high critical temperature may yield more turbine net power output and a better thermal efficiency. The relation between critical temperature and system performance as outlined in the present work agrees with the results and analyses in Refs. [33,51,52]. On the other hand, Fig. 10 (b) shows

that there is no clear relationship between the critical pressure of the working fluid and system performance.

3.6. Exergy loss analysis

Exergy loss analysis is important to explore the dissipation of usable energy in the ORC components due to irreversibilities. Such an analysis was carried out for each component of the present ORC system under the operating conditions where the highest thermal and exergy efficiencies were reached. Fig. 11 shows that the highest exergy loss occurred in the evaporator (HE) due to the irreversibility during heat transfer between Therminol 66 and the working fluid. The percentage of exergy loss was 55.4%, 53.6%, 51.7% and 50.4% adopting butane, pentane, cyclopentane and MM, respectively. The results agree with the analyses of Li et al. [53] and Safarian et al. [54], who reported that the highest exergy loss occurs in the evaporator which represents the critical component of regular ORC systems. Other practical works [9,15] that looked at the exergy loss in ORC systems also found that the largest contribution is exerted in the evaporator. The exergy loss in the evaporator using butane or pentane with a heat source temperature in the range of 180-230 °C is lower than when using cyclopentane or MM with a heat source temperature of 280 °C. Working fluids with a high critical temperature can provide a high turbine inlet temperature and evaporation temperature. Moreover, they allow for a better matching between the heating cycle and working fluid in the evaporator at higher temperatures. This explains the large exergy loss in the evaporator when adopting butane or pentane in comparison to cyclopentane or MM. In this context, butane for a heat source temperature of 180 °C had a larger difference between the heat source temperature and the turbine inlet temperature and more exergy loss in the evaporator, while MM had a smaller difference and less exergy loss.

The results attribute the low thermal efficiency to the poor turbine efficiency, as it generates less power output in relation to the available enthalpy difference. Using a turbine with a better efficiency would increase the thermal efficiency and performance of the ORC system. In general, the present ORC system may be effective for recovering heat from wide range of heat sources, especially since the market needs to introduce small units to recover heat from various sources.

4. Conclusions and outlook to future work

An ORC system was experimentally investigated utilizing electrical heaters as a heat source. System performance in terms of thermal efficiency and exergy efficiency was studied over a wide range of heat source temperature, turbine inlet pressure and superheating degree by using butane, pentane, cyclopentane or MM as a working fluid. The heat source temperature was in the range of 80-180 °C for butane, 130-230 °C for pentane, 180-280 °C for cyclopentane and 180-280 °C for MM. The turbine inlet pressure was in the range of 28-36 bar for butane, 24-32 bar for pentane, 36-44 bar for cyclopentane and 10-18 bar for MM. The maximum measured values of thermal efficiency and exergy efficiency were 8.0% and 25.2%, respectively, and were found for MM. The maximum turbine efficiency and enthalpy drop across the turbine were 53.5% and 48.8 kJ/kg adopting MM as a working fluid. With a superheating degree from 3 to 6°C, all working fluids reached the highest thermal and exergy efficiencies. Moreover, a pressure ratio between 0.88-0.91 was optimal throughout. The results show that a small degree of superheating is efficient to increase system performance. An exergy loss analysis indicated that the highest exergy loss occurred in the evaporator due to the irreversibility during heat transfer from the heat source. In addition, it was confirmed that working fluids with a high critical temperature are more beneficial for ORC systems with a heating cycle.

This work aims to provide experimental data that can be employed to improve and optimize ORC systems. The low turbine efficiency during the present operations clearly indicates that a new dedicated turbine must be designed to enhance power output. Moreover, we are interested to experimentally investigate low-GWP refrigerants as working fluids. Future work will include the heat transfer properties of the system, i.e. pinch point temperature difference, heat recovery efficiency and heat exchanger performance.

Acknowledgements

The authors acknowledge the financial support by the German Academic Exchange Service (DAAD). We thank Dr. Gerhard Herres, University of Paderborn who provided insight and expertise that greatly assisted the present work.

Nomenclature

c_p	Specific isobaric heat capacity [kJ/(kg K)]
$\dot{E}^{in}$	Exergy flow input [kW]
H	Specific enthalpy [kJ/kg]
$\dot{I}$	Exergy flow loss [kW]
$\dot{m}$	Mass flow rate in ORC [kg/s]
$\dot{m}_{HC}$	Mass flow rate in heating cycle [kg/s]
M	Molar mass [g/mol]
p_c	Critical pressure [bar]
$\dot{Q}$	Heat flow [kW]
$\dot{Q}_{HC}$	Heat flow in heating cycle [kW]
S	Specific entropy [kJ/(kg K)]
T_c	Critical temperature [°C]
$\dot{W}_{net}$	Net power output [kW]
$\dot{W}_P$	Pump power [kW]
$\dot{W}_T$	Turbine power output [kW]

Acronyms

GWP	Global warming potential [-]
HC	Heating cycle [-]
HE	Heat exchanger [-]
HT	High-temperature [-]
LT	Low-temperature [-]
ODP	Ozone depletion potential [-]
TIP	Turbine inlet pressure [bar]

Greek symbols

η_{ex}	Exergy efficiency [%]
η_t	Isentropic turbine efficiency [%]
η_{th}	Thermal efficiency [%]

Subscripts and Superscripts

1-2	Process from state 1 to state 2
C	Condenser [-]
G	Generator [-]
M0	Heating cycle pump [-]
M1	ORC pump [-]
M2	Cooling cycle pump [-]
X_i	Exergy loss percentage [%]

References

[1] Khan I., Hou F, Irfan M, Zakari A, Le H P. Does energy trilemma a driver of economic growth? The roles of energy use, population growth, and financial development. Renewable and Sustainable Energy Reviews 2021;146:111157. https://doi.org/10.1016/J.RSER.2021.111157.

[2] Majeed M T, Ozturk I, Samreen I, Luni T. Evaluating the asymmetric effects of nuclear energy on carbon emissions in Pakistan. Nuclear Engineering and Technology 2022;54:1664–1673. https://doi.org/10.1016/j.net.2021.11.021.

[3] Shi Y, Lin R, Wu X, Zhang Z, Sun P, Xie L, Su H. Dual-mode fast DMC algorithm for the control of ORC based waste heat recovery system. Energy 2022;244:122664. https://doi.org/10.1016/j.energy.2021.122664.

[4] Wieland C, Dawo F, Schifflechner C, Astolfi M. Market Report on organic Rankine cycle power system: Recent development and outlook. In 6th International Seminar on ORC Power Systems, October 11-13, 2021, Munich, Germany. https://orc-world-map.org.

[5] Tartière T, Astolfi, M. A World Overview of the Organic Rankine Cycle Market. Energy Procedia 2017:129;2–9. https://doi.org/10.1016/J.EGYPRO.2017.09.159.

[6] Fatigati F, Vittorini D, di Bartolomeo M,Cipollone R. Experimental characterization of a small-scale solar Organic Rankine Cycle (ORC) based unit for domestic microcogeneration. Energy Conversion and Management 2022;258. https://doi.org/10.1016/j.enconman.2022.115493.

[7] Park BS, Usman M, Imran M, Pesyridis A. Review of Organic Rankine Cycle experimental data trends. Energy Conversion and Management 2018;173:679–691. https://doi.org/https://doi.org/10.1016/j.enconman.2018.07.097.

[8] Mascuch J, Novotny V, Vodicka V, Spale J, Zeleny Z. Experimental development of a kilowatt-scale biomass fired micro – CHP unit based on ORC with rotary vane expander. Renewable Energy 2020;147:2882–2895. https://doi.org/10.1016/j.renene.2018.08.113.

[9] Feng Y, Wang X, Niaz H, Hung T, He Z, Jahan Z A, & Xi, H. Experimental comparison of the performance of basic and regenerative organic Rankine cycles. Energy Conversion and Management 2020;223:113459. https://doi.org/10.1016/J.ENCONMAN.2020.113459.

[10] Gao W, Wu Z, Tian Z, Zhang Y. Experimental investigation on an R290-based organic Rankine cycle utilizing cold energy of liquid nitrogen. Applied Thermal Engineering 2022;202:117757. https://doi.org/10.1016/J.APPLTHERMALENG.2021.117757.

[11] Wang F, Gao W, Li G, Tian Z,Wang, X. Experimental study on power generation plant of a 1 kW small-scale Organic Rankine Cycle system using R290. Energy Science and Engineering 2022;10:740–751. https://doi.org/10.1002/ese3.1049.

[12] Araya S, Wemhoff A P, Jones G F, Fleischer A S. An experimental study of an Organic Rankine Cycle utilizing HCFO-1233zd(E) as a drop-in replacement for HFC-245fa for ultra-low-grade waste heat recovery. Applied Thermal Engineering 2020;180:115757. https://doi.org/10.1016/J.APPLTHERMALENG.2020.115757.

[13] Zygmunt Kaczmarczyk T. Experimental research of a small biomass organic Rankine cycle plant with multiple scroll expanders intended for domestic use. Energy Conversion and Management 2021;244: https://doi.org/10.1016/j.enconman.2021.114437.

[14] İpek O, Mohammedsalih, M M, Gürel B, Kılıç B. Experimental investigation of low-temperature organic Rankine cycle using waste heat from gas turbine bearings for different conditions. International Journal of Environmental Science and Technology 2022; 19:1519–1530. https://doi.org/10.1007/s13762-021-03172-x.

[15] Wu T, Wei X, Meng X, Ma X., Han J. Experimental study of operating load variation for organic Rankine cycle system based on radial inflow turbine. Applied Thermal Engineering 2020;166:114641. https://doi.org/10.1016/J.APPLTHERMALENG.2019.114641.

[16] Qiu, K, Entchev E. A micro-CHP system with organic Rankine cycle using R1223zd(E) and n-Pentane as working fluids. Energy 2022;239:121826. https://doi.org/10.1016/J.ENERGY.2021.121826.

[17] Carraro G, Bori V, Lazzaretto A, Toniato G, Danieli P. Experimental investigation of an innovative biomass-fired micro-ORC system for cogeneration applications. Renewable Energy 2020;161:1226–1243. https://doi.org/10.1016/J.RENENE.2020.07.012.

[18] Qiu K, Entchev E. Development of an organic Rankine cycle-based micro combined heat and power system for residential applications. Applied Energy 2020;275:115335. https://doi.org/10.1016/J.APENERGY.2020.115335.

[19] Linnemann M, Priebe KP, Heim A, Wolff C, Vrabec J. Experimental investigation of a cascaded organic Rankine cycle plant for the utilization of waste heat at high and low temperature levels. Energy Conversion and Management 2020;205:112381. https://doi.org/10.1016/j.enconman.2019.112381.

[20] Zhou N, Wang X, Chen Z, Wang Z. Experimental study on Organic Rankine Cycle for waste heat recovery from low-temperature flue gas. Energy 2013;55:216–225. https://doi.org/10.1016/j.energy.2013.03.047.

[21] Allweiler GmbH. Product catalog Allweiler NTWH 25 200/10. Website address: https://www.allweiler.de/16550/Products/Product-Catalog/Centrifugal-Pumps/with-shaft-seal/Base-plate-design/ALLHEAT-NTWH/Product/awr_index_2017.aspx.; accessed on 20th April 2022.

[22] Dubberke F, Linnemann M, Abbas W K, Baumhögger E, Priebe KP, Roedder M, Neef, M, Vrabec J. Experimental setup of a cascaded two-stage organic Rankine cycle. Applied Thermal Engineering 2018;131:958–964. https://doi.org/10.1016/j.applthermaleng.2017.11.137.

[23] Netzsch Group. Products-and-accessories. NETZSCH NEMO. Website address: https://pumps-systems.netzsch.com/en/products-and-accessories/nemo-progressing-cavity-pumps.; accessed on 20th April 2022.

[24] Vahterus Company. Plate and shell heat exchangers. Website address: https://vahterus.com/technology/customised-pshe-solution/fully-welded-design. ; accessed on 20th April 2022.

[25] Abbas WKA, Linnemann M, Baumhögger E, Vrabec J. Experimental study of two cascaded organic Rankine cycles with varying working fluids. Energy Conversion and Management 2021;230:113818. https://doi.org/10.1016/j.enconman.2020.113818.

[26] Abbas WKA, Vrabec J. Cascaded dual-loop organic Rankine cycle with alkanes and low global warming potential refrigerants as working fluids. Energy Conversion and Management 2021;249:114843. https://doi.org/10.1016/J.ENCONMAN.2021.114843.

[27] Fragol company. Product data sheet Therminol 66. Website address: http://www.fragol.de.asp; accessed on 20th December 2021.

[28] Hu B, Guo J, Yang Y, Shao Y. Selection of working fluid for organic Rankine cycle used in low temperature geothermal power plant. Energy Reports 2022;8:179–186. https://doi.org/10.1016/j.egyr.2022.01.102.

[29] Wang, S., Liu, C., Zhang, S., Li, Q., & Huo, E. (2022). Multi-objective optimization and fluid selection of organic Rankine cycle (ORC) system based on economic-environmental-sustainable analysis. Energy Conversion and Management, 254, 115238. https://doi.org/10.1016/J.ENCONMAN.2022.115238.

[30] Dai X, Shi L, Qian W. Review of the Working Fluid Thermal Stability for Organic Rankine Cycles. Journal of Thermal Science 2019;28:597–607. https://doi.org/10.1007/s11630-019-1119-3.

[31] Wang, W., Dai, X., & Shi, L. (2022). Influence of thermal stability on organic Rankine cycle systems using siloxanes as working fluids. Applied Thermal Engineering 2022;200:117639. https://doi.org/10.1016/J.APPLTHERMALENG.2021.117639.

[32] Li Y, Li W, Gao X, Ling X. Thermodynamic analysis and optimization of organic Rankine cycles based on radial-inflow turbine design. Applied Thermal Engineering 2021;184:116277. https://doi.org/10.1016/J.APPLTHERMALENG.2020.116277.

[33] Uusitalo A, Honkatukia J, Turunen-Saaresti, T, Grönman A. Thermodynamic evaluation on the effect of working fluid type and fluids critical properties on design and performance of Organic Rankine Cycles. Journal of Cleaner Production 2018;188: 253–263. https://doi.org/10.1016/J.JCLEPRO.2018.03.228.

[34] Loni R, Mahian O, Markides C N, Bellos E, le Roux, W G, Kasaeian A, Najafi G, Rajaee F. A review of solar-driven organic Rankine cycles: Recent challenges and future outlook. Renewable and Sustainable Energy Reviews 2021;150:111410. https://doi.org/10.1016/J.RSER.2021.111410.

[35] Sorgulu F, Akgul M B, Cebeci E, Yilmaz T O, Dincer I. A new experimentally developed integrated organic Rankine cycle plant. Applied Thermal Engineering 2021;187:116561. https://doi.org/10.1016/J.APPLTHERMALENG.2021.116561.

[36] Bahrami M, Pourfayaz F, Kasaeian A. Low global warming potential (GWP) working fluids (WFs) for Organic Rankine Cycle (ORC) applications. In Energy Reports 2022;8:2976–2988. Elsevier Ltd. https://doi.org/10.1016/j.egyr.2022.01.222.

[37] Pili R, Bojer Jørgensen S, Haglind F. Multi-objective optimization of organic Rankine cycle systems considering their dynamic performance. Energy;2022;246:123345. https://doi.org/10.1016/J.ENERGY.2022.123345.

[38] Braimakis K, Karellas S. Exergetic optimization of double stage Organic Rankine Cycle (ORC). Energy 2018;149;296–313. https://doi.org/10.1016/j.energy.2018.02.044.

[39] Uusitalo A, Turunen-Saaresti T, Honkatukia J, Dhanasegaran R. Experimental study of small scale and high expansion ratio ORC for recovering high temperature waste heat. Energy 2020;208:118321. https://doi.org/10.1016/J.ENERGY.2020.118321.

[40] Aljundi IH. Effect of dry hydrocarbons and critical point temperature on the efficiencies of organic Rankine cycle, Renew. Energy 2011;36:1196–1202. https://doi.org/10.1016/j.renene.2010.09.022.

[41] Barse KA, Mann MD. Maximizing ORC performance with optimal match of working fluid with system design, Applied Thermal Engineering 2016;100:11–19. https://doi.org/10.1016/j.applthermaleng.2016.01.167.

[42] Vivian J, Manente G, Lazzaretto A. A general framework to select working fluid and configuration of ORCs for low-to-medium temperature heat sources, Appl. Energy 2015;156:727–746. https://doi.org/10.1016/j.apenergy.2015.07.005.

[43] Zhai H, An Q, L. Shi. Analysis of the quantitative correlation between the heat source temperature and the critical temperature of the optimal pure working fluid for subcritical organic Rankine cycles, Applied Thermal Engineering 2016;99:383–391. http://doi.org/10.1016/j.applthermaleng.2016.01.058.

[44] Lemmon EW, Huber ML, McLinden MO. Reference fluid thermodynamic and transport properties (REFPROP), version 10.0, in NIST Standard Reference Database 23. National Institute of Standard and Technology, Gaithersburg, MD, 2007.

[45] Bücker D, Wagner W. Reference equations of state for the thermodynamic properties of fluid phase n-butane and isobutane, J. Phys. Chem. Ref. Data 2006;35:929–1019. https://doi.org/10.1063/1.1901687.

[46] Span R, Wagner W. Equations of State for Technical Applications. II. Results for Nonpolar Fluids. In International Journal of Thermophysics 2003;24:41-109. https://doi.org/10.1023/A:1022310214958.

[47] Gedanitz H, Davila MJ, Lemmon EW. Speed of sound measurements and a fundamental equation of state for cyclopentane, J. Chem. Eng. Data 2015;60:1331–1337. https://doi.org/10.1021/je5010164.

[48] Thol M, Dubberke F, Rutkai G, Windmann T, Köster A, Span R, Vrabec J. Fundamental equation of state correlation for hexamethyldisiloxane based on experimental and molecular simulation data. Fluid Phase Equilibria 2016;418:133–151. https://doi.org/10.1016/J.FLUID.2015.09.047.

[49] Zhang T, Liu L, Hao J, Zhu T, Cui G. Correlation analysis based multi-parameter optimization of the organic Rankine cycle for medium- and high-temperature waste heat recovery. Applied Thermal Engineering 2021;188.https://doi.org/10.1016/j.applthermaleng.2021.116626.

[50] Mahian O, Mirzaie M R, Kasaeian A, Mousavi S H. Exergy analysis in combined heat and power systems: A review. Energy Conversion and Management 2020;226:113467. https://doi.org/10.1016/J.ENCONMAN.2020.113467.

[51] Shu G, Li X, Tian H, Liang X, Wie H, Wang X. Alkanes as working fluids for high-temperature exhaust heat recovery of diesel engine using organic Rankine cycle. Applied Energy 2014;119:204–217. https://doi.org/10.1016/j.apenergy.2013.12.056.

[52] Liu P, Shu G, Tian H, Wang X, Yu Z. Alkanes based two-stage expansion with interheating Organic Rankine cycle for multi-waste heat recovery of truck diesel engine. Energy 2018;147;337–350. https://doi.org/10.1016/j.energy.2017.12.109.

[53] Li W, Feng X, Yu LJ, Xu J. Effects of evaporating temperature and internal heat exchanger on organic Rankine cycle. Applied Thermal Engineering 2011;31:4014–4023. https://doi.org/10.1016/J.APPLTHERMALENG.2011.08.003.

[54] Safarian S, Aramoun F. Energy and exergy assessments of modified Organic Rankine Cycles (ORCs). Energy Reports 2015; 1:1–7. https://doi.org/10.1016/j.egyr.2014.10.003.

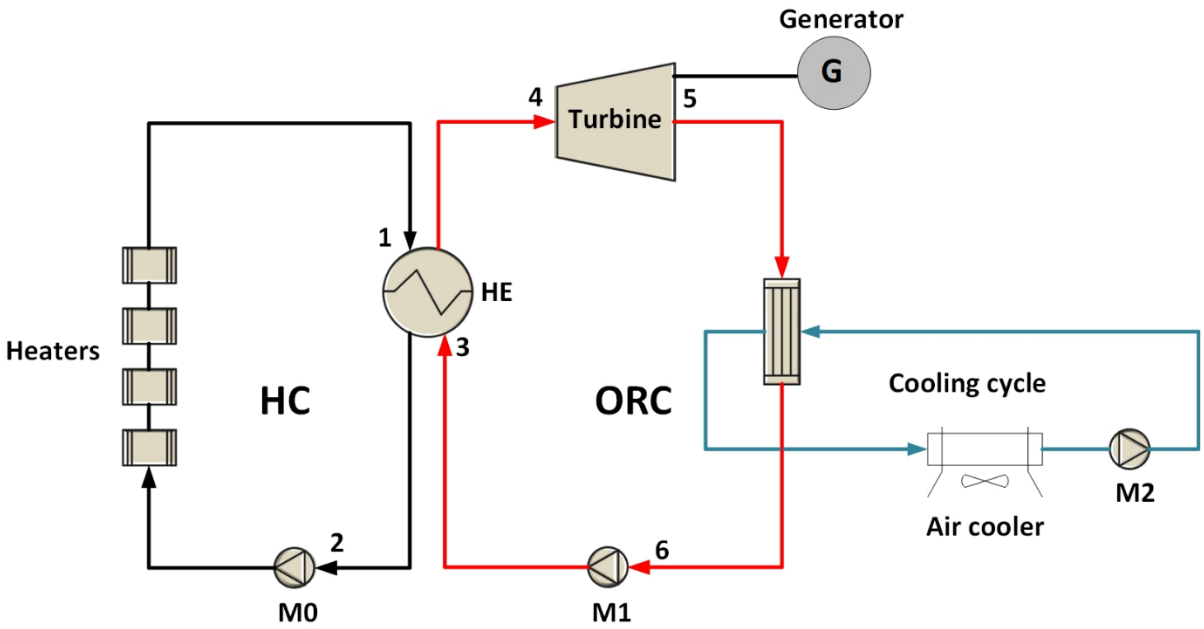

Fig. 1. Layout of the investigated ORC test rig in the present work.

(a)

(b)

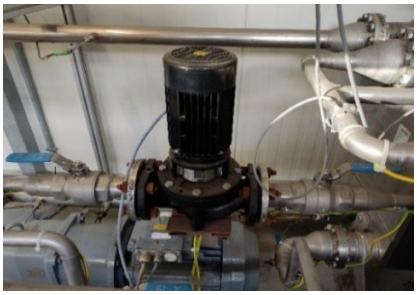

(c)

(d)

(e)

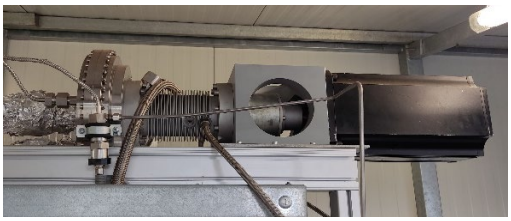

(f)

(g)

Fig. 2. (a) The ORC test rig was in a container due to safety considerations, (b) air cooler, (c) pump M2, (d) condenser C, (e) heat exchanger HE, (f) turbine T and generator G, (g) pump M0.

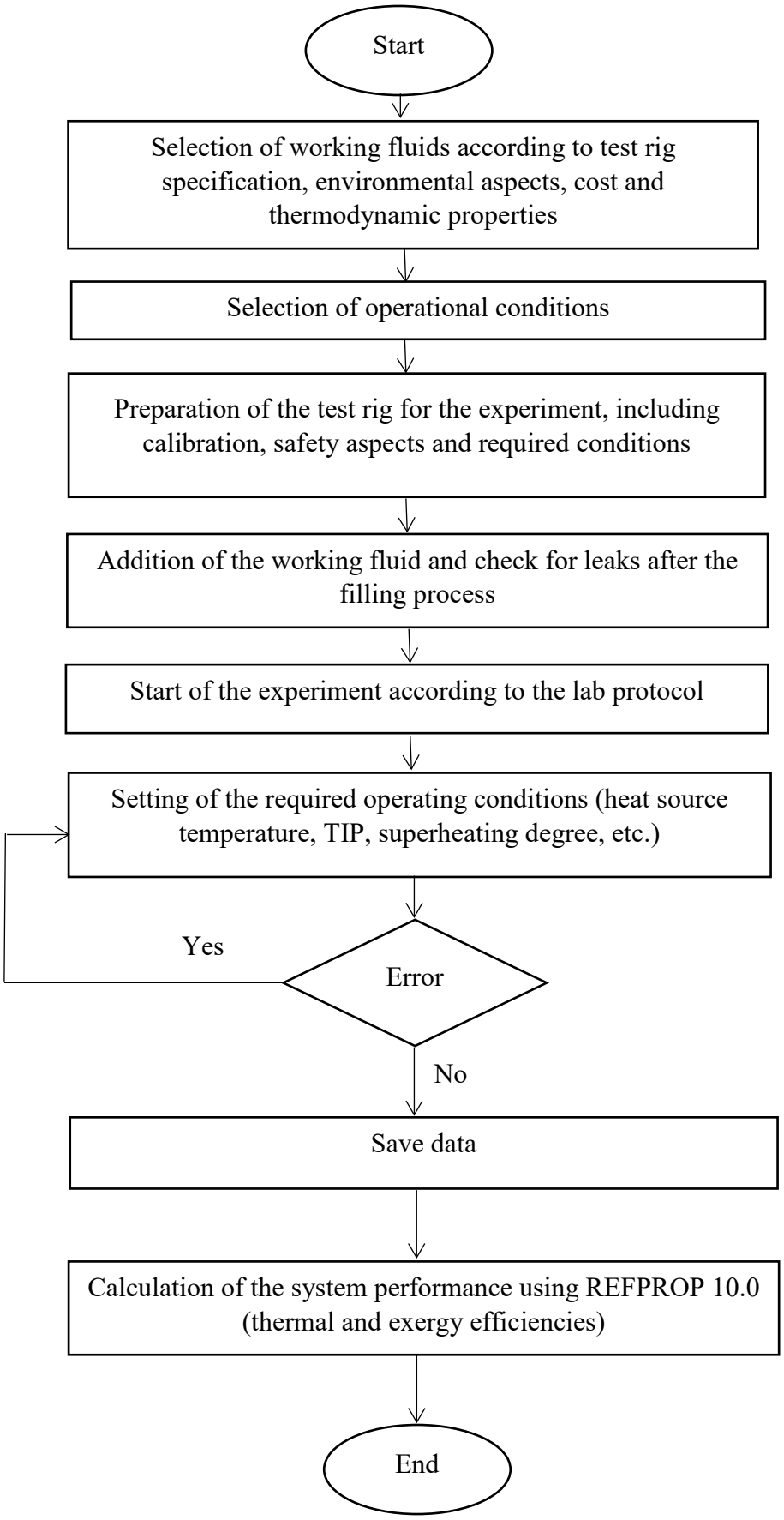

Fig. 3. Procedure of the experimental work.

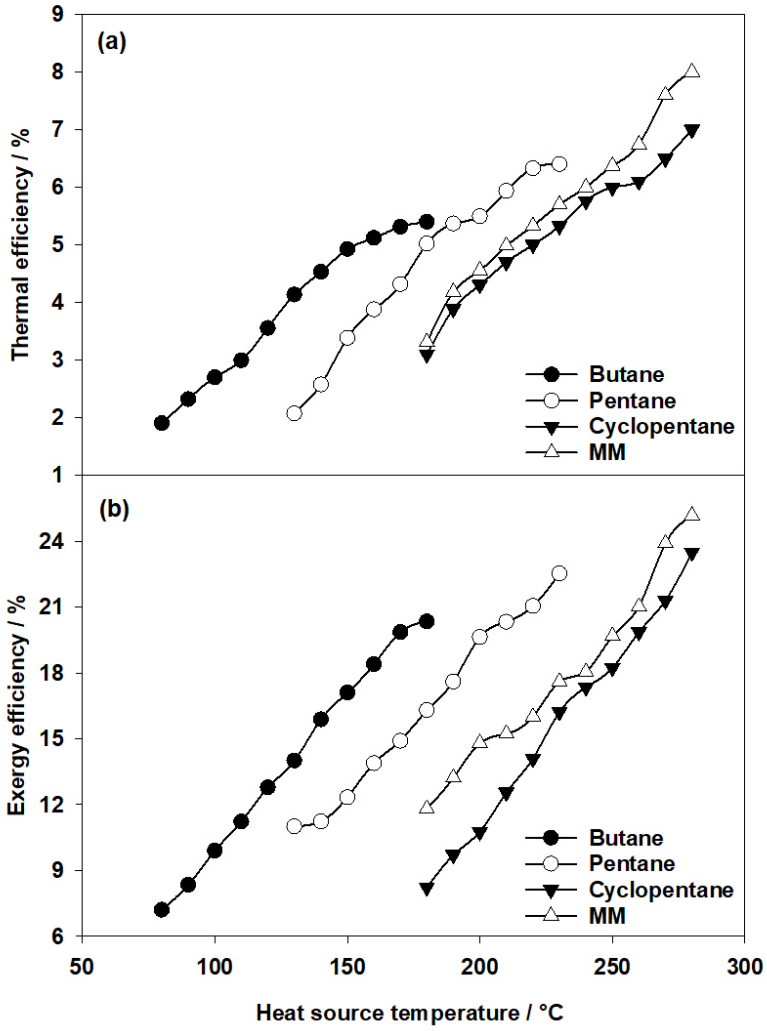

Fig. 4. Effect of heat source temperature on (a) thermal efficiency and (b) exergy efficiency for varying working fluids.

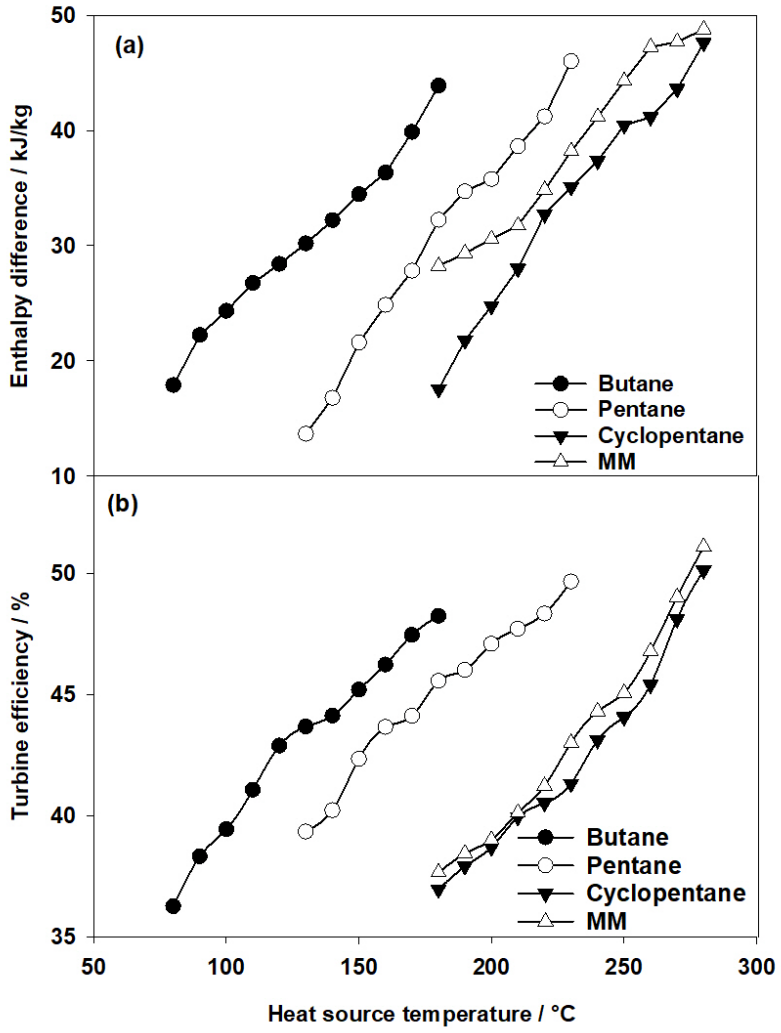

Fig. 5. (a) Enthalpy difference and (b) turbine efficiency as a function of heat source temperature for varying working fluids.

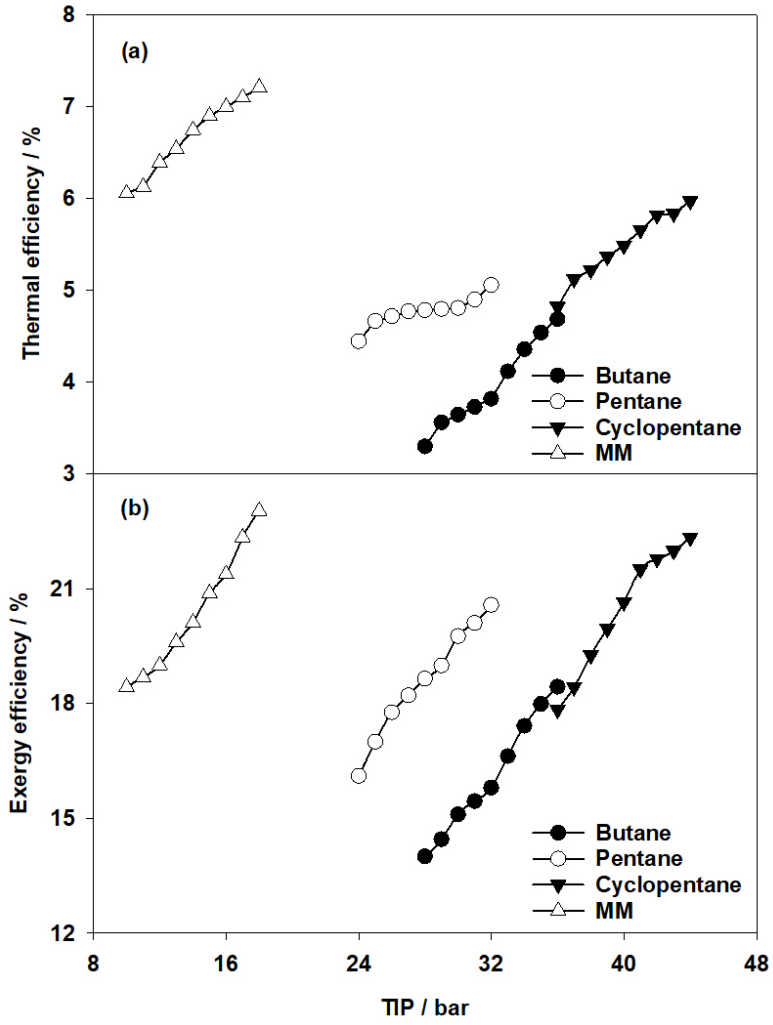

Fig. 6. Effect of turbine inlet pressure on (a) thermal efficiency and (b) exergy efficiency for varying working fluids.

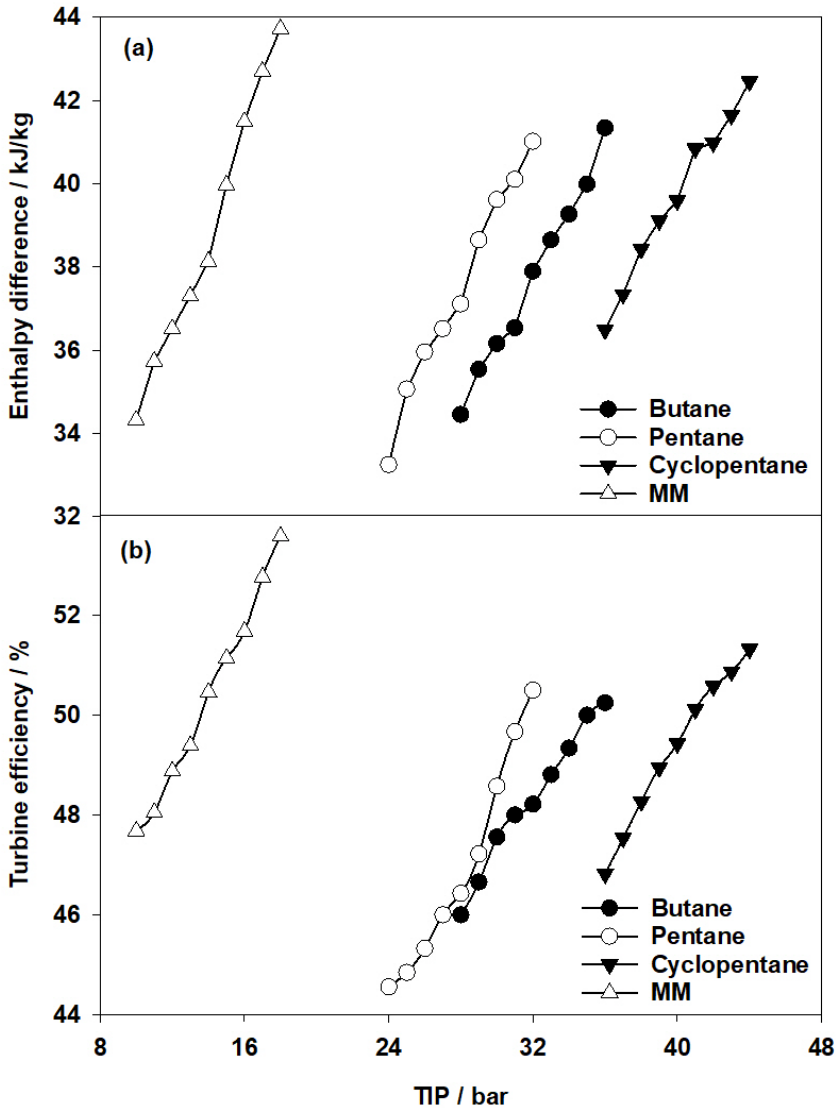

Fig. 7. Variation of (a) enthalpy difference and (b) turbine efficiency with turbine inlet pressure for varying working fluids.

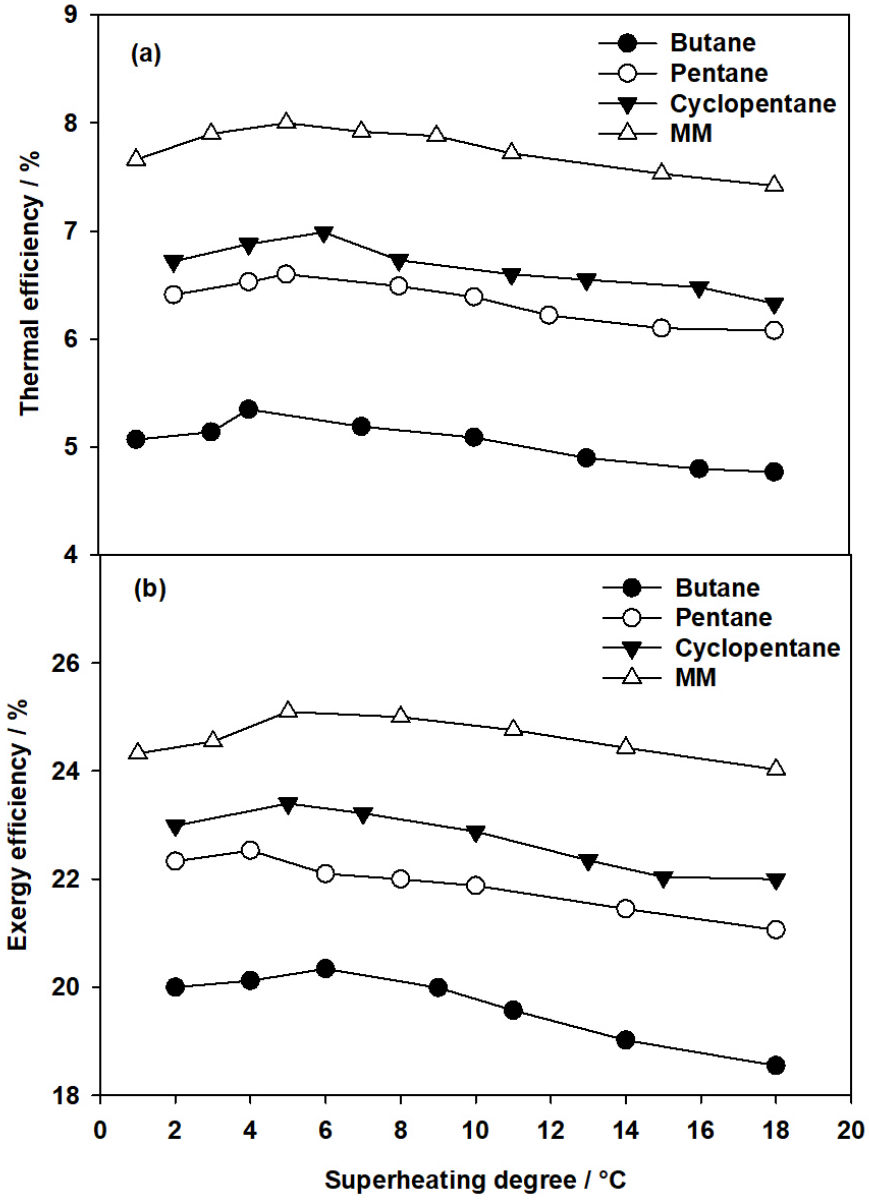

Fig. 8. (a) Thermal efficiency and (b) exergy efficiency as a function of superheating degree for varying working fluids.

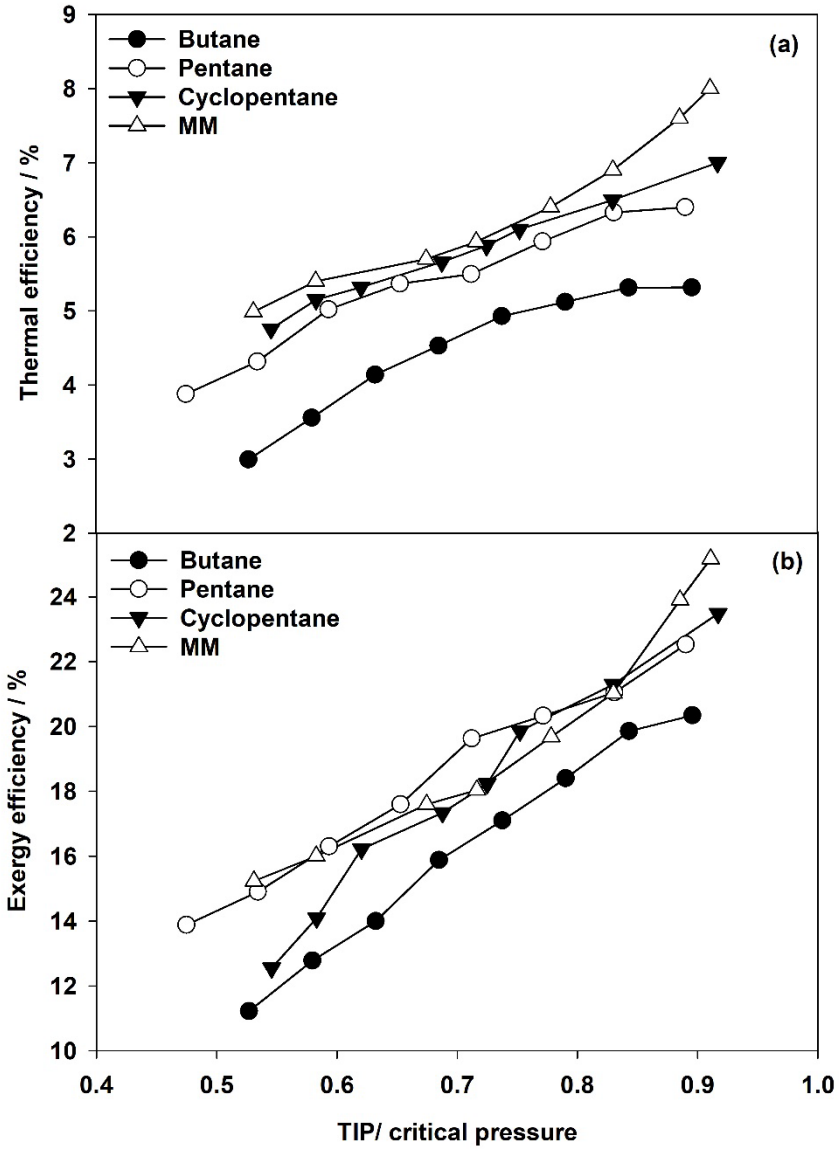

Fig. 9. Variation of (a) thermal efficiency and (b) exergy efficiency with pressure ratio for varying working fluids.

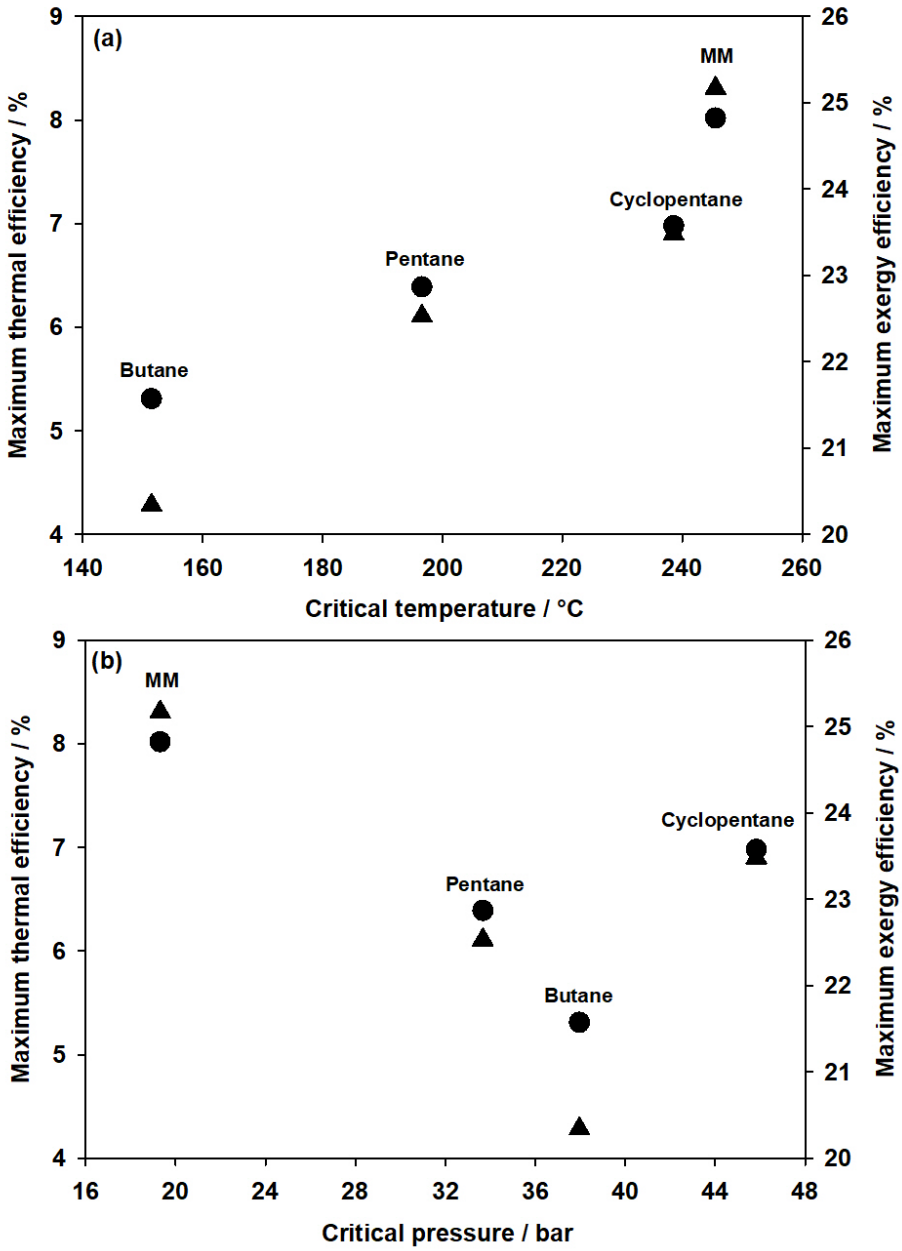

Fig. 10. Maximum thermal efficiency (bullets) and maximum exergy efficiency (triangles) over (a) critical temperature and (b) critical pressure for varying working fluids.

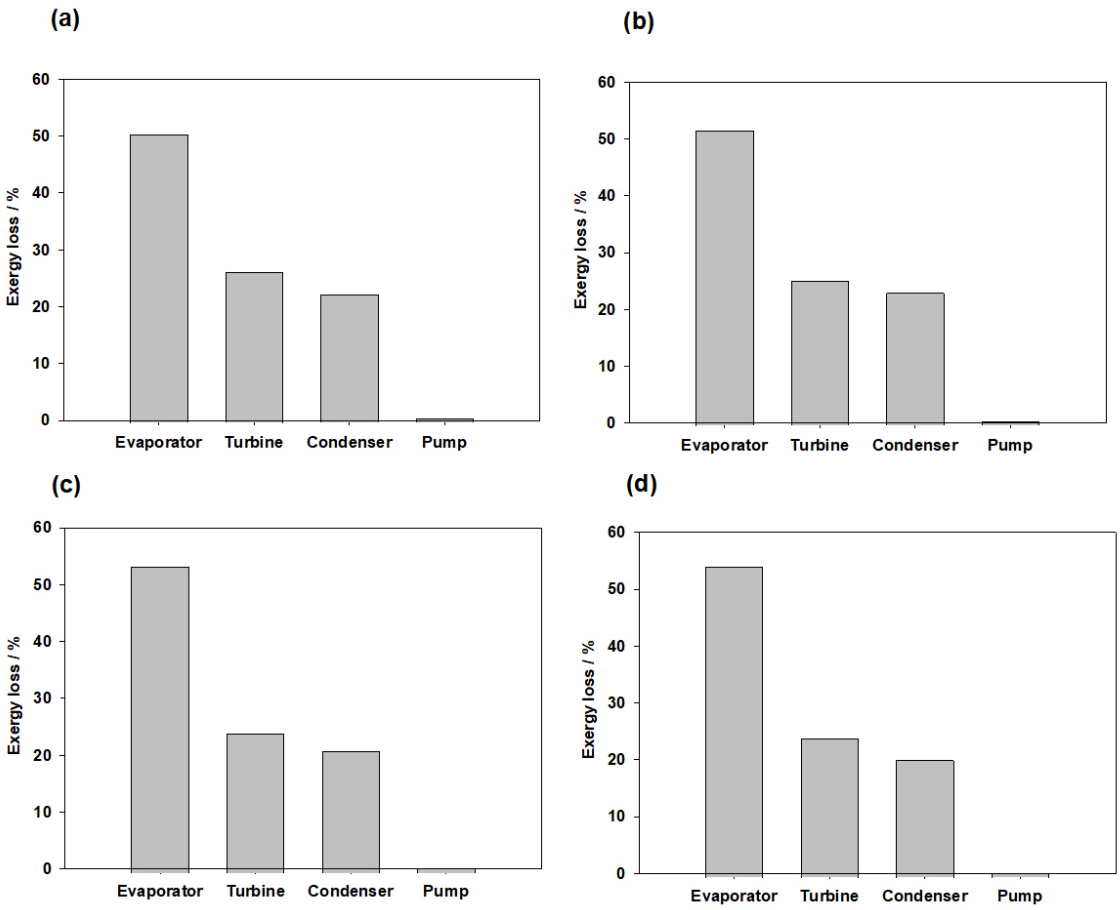

Fig. 11. Percentage of exergy loss in the main ORC components using (a) MM, (b) cyclopentane, (c) pentane and (d) butane as a working fluid.

Table 1: Overview of recent experimental studies of the ORC.

Ref.	Working fluid	Operating conditions	η_{th}[%]	η_t[%]
[8]	MM	192 °C	2.5%	28%-52%
[9]	R245fa	77-108 °C	5.5%	
[10]	R290	n.a	6.7%	
[11]	R290	20-55 °C	6.49%	
[12]	R1223zd(E) & R245fa	85.7°C	5.0%	
[13]	HFE7100	n.a	6.5%	52-71%
[14]	R134a	86-88 °C	6.84%	
[15]	R245fa	120 °C	2.54%	
[6]	R245fa	70-110 °C	4-6%	
[16]	R1223zd(E) n-pentane	135-136°C	5.6-5.3%	
[17]	R245fa	120-155°C	7.4%	57%

Table 2: Main components of the ORC system considered in the present work.

Component	Type	Range	Refs.
M0	Radial flow	Up to: 350 °C, 1250 m^3/h	[21]
Flow heaters	GC heat D01-00508	0 – 158 kW	[22]
M1	NETZSCH NEMO	-20 – 200 °C	[23]
HE	Plate & Shell	-20 – 280 °C, -1 – 60 bar	[24]
C	Plate heat exchanger	Max. 25 bar, -195 – 195 °C	[22]
Turbine	Radial flow	Up to 325 °C	[22]
Generator	6-pole servomotor	Up to 15 kW	[22]

Table 3: Measuring devices of the ORC test rig.

Variable	Sensor type	Range	Uncertainty
p (HC)	Jumo	0 – 6 bar	± 0.5%
T_1, T_2 (HC)	Pt 1000	-40 – 380 °C	± 0.1%
$\dot{m}_{HC}$ (HC)	Pressure difference	0 – 25 bar	± 0.1%
T_3, T_4	Pt 1000	-40 – 380 °C	± 0.1%
T_5, T_6	Pt 1000	-40 – 250 °C	± 0.1%
p_3, p_4	APT	0 – 60 bar	± 0.5%
p_5, p_6	APT	0 – 16 bar	± 0.5%
$\dot{m}$	Pressure difference	0 – 100 bar	≤ 0.065 %

Table 4: Working fluids and their properties.

Working fluid	T_c (°C)	p_c (bar)	M (g/mol)	GWP	ODP	Refs.
MM	245.55	19.311	162.38	Very low	0	[51,55]
Cyclopentane	238.57	45.828	70.133	~20	0	[46,50]
Pentane	196.55	33.675	72.149	~20	0	[46,49]
Butane	151.98	37.96	58.122	4	0	[46,48]

Table 5: Parameters and operational conditions.

Parameter	Range
Effects of heat source analysis	
Heat source temperature	80 – 280 °C
Mass flow rate (ORC)	0.08 – 0.12 kg/s
Ambient pressure	1.013 bar
Ambient temperature	5 – 25 °C
Mass flow rate (HC)	0.42 – 0.55 kg/s
Effects of turbine inlet pressure	
Turbine inlet pressure	10 – 44 bar
Mass flow rate (ORC)	0.09 – 0.14 kg/s
Mass flow rate (HC)	0.37 – 0.56 kg/s
Effects of superheating degree	
Superheating degree	1 – 18 °C
Mass flow rate (ORC)	0.08 – 0.12 kg/s
Mass flow rate (HC)	0.45 – 0.55 kg/s

Table 6: Comparison of present results with the literature.

Working fluid	Parameter [%]	Temperature [°C]	This work	Ref.	Difference
Pentane	η_{th}	136	5.38%	5.3 % [16]	0.08
Butane	η_{th}	180	5.4%	5.51% [26]	0.11